Asymmetric Swing-leg Motions for Speed-up of Biped Walking

doi: https://doi.org/10.20965/jrm.2017.p0490

Paper: Rb*--**-****:**

Asymmetric Swing-leg Motions for Speed-up of Biped Walking

Yuta Hanazawa[1] and Fumihiko Asano[2]

[1]Dept. of Applied Science for Integrated System Engineering, Graduate School of Engineering, Kyushu Institute of Technology, 1-1 Sensui, Tobata, Kitakyushu, Fukuoka 804-8550, JAPAN.
E-mail: hanazawa-y@ise.kyutech.ac.jp
[2]School of Information Science, Japan Advanced Institute of Science and Technology, 1-1 Asahidai, Nomi, Ishikawa 923-1292, JAPAN.
E-mail: fasano@jaist.ac.jp
[Received 00/00/00; accepted 00/00/00]

Abstract. This study presents a novel swing-leg control strategy for speed-up of biped robot walking. The trajectory of tip of the swing-leg is asymmetric at the center line of the torso in the sagittal plane for this process. A methodology is proposed enables robots to achieve synchronized the asymmetric swing-leg motions with the stance-leg angle to accelerate their walking speed. The effectiveness of the proposed method was simulated using numerical methods.

Keywords: Biped robot, Limit cycle, Asymmetric motion

1. INTRODUCTION

Biped robots have high-performance movement, and they can capacity to walk on various types of terrain [1], [2]. Moreover, they are able to change their walking direction in confined spaces. It is considered that biped robots ultimately have the potential to move with the same walking characteristics as humans. Biped robots development has achieved stability for dynamic walking: however, the walking movements of biped robots consume a large amount of energy. Collins et al. have shown that the energy consumption for the walking movements for ASIMO is approximately 30 times higher than that for the walking movements of a human [3]. When the biped robots achieve high-speed walking, the energy consumption is increased.

To achieve energy-efficient and high-speed for biped robots, we have studied biped walking based on a passive dynamic walking model [4]. This type of walking is frequently called limit cycle walking [5]. Typically, limit cycle walking robots achieve energy-efficient but slow dynamic walking [6], [7], [8], [9].

Recent approaches to achieve variable speed for limit cycle walking have been studied. Narukawa et al. demonstrated limit cycle walking using torso effects [10]. Asano et al. and Kinugasa et al. demonstrated limit cycle walking using telescopic-leg effects [11], [12]. Hanazawa et al.demonstrated limit cycle walking using an up-and-down wobbling mass and swinging-arm effects [13], [14].

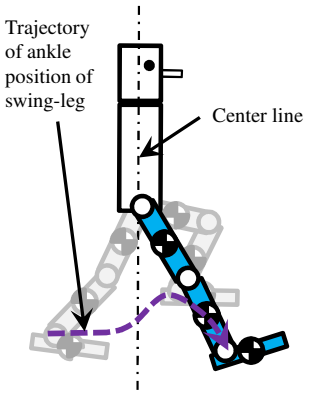

Fig. 1. Schematic for swing-leg motion during dynamic walking

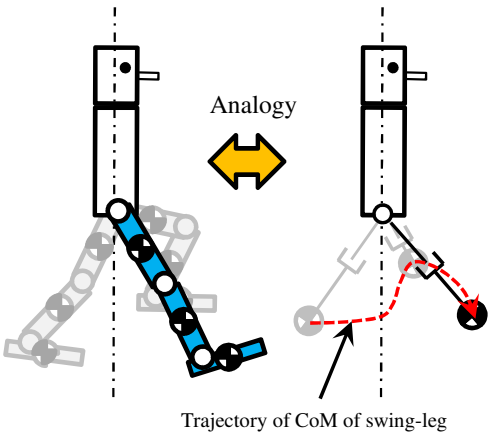

Fig. 2. Analogy between swing-leg motion and up-and-down motion of mass

In this study, we elaborate the asymmetric swing-leg motion in walking to improve the walking speed for limit cycle walking of biped robots. Asymmetric swing-leg motion is considered important for dynamic walking. To demonstrate this mechanism, an analogy was introduced as shown in Fig. 2. The swing-leg was replaced with a telescopic mass. Using this simplification, the effects of ths asymmetric swing-leg motion can be clearly investigated. Moreover, we propose that biped robots can achieve speed-up of dynamic walking by using asymmet-

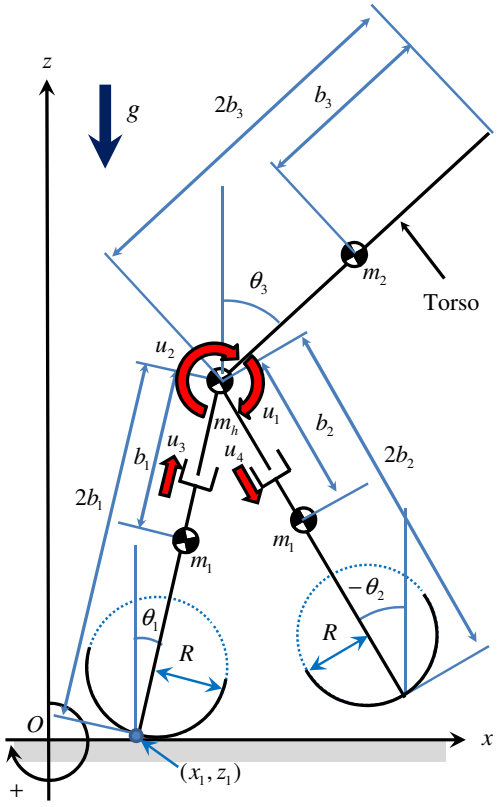

Fig. 3. Model of telescopic-legged biped robot with arc-feet and torso

ric swing-leg motion.

2. MODEL OF BIPED ROBOT

2.1. Dynamic equation

Fig. 3 shows the biped robot walking model used for the numerical method simulations. This robot has telescopic legs like previous robots [12], [15]. The robot has two linear actuators for control of their telescopic legs and two rotational actuators for control of their torso angle and swing-leg. The dynamic equation of the robot is given by

$$\boldsymbol{M}(\boldsymbol{q})\ddot{\boldsymbol{q}}+\boldsymbol{H}(\boldsymbol{q},\dot{\boldsymbol{q}})=\boldsymbol{S}_1\boldsymbol{u}+\boldsymbol{J}_c(\boldsymbol{q})^{\mathrm{T}}\boldsymbol{\lambda}, \quad \ldots\ldots (1)$$

where $\boldsymbol{q}=[\theta_1,\ \theta_2,\ \theta_3,\ b_1,\ b_2,\ x_1,\ z_1]^{\mathrm{T}}$ is the generalized coordinate vector, $\boldsymbol{M}(\boldsymbol{q})\in\mathbb{R}^{7\times7}$ is the inertia matrix, $\boldsymbol{H}(\boldsymbol{q},\dot{\boldsymbol{q}})\in\mathbb{R}^7$ is the vector that consists of the Coriolis, centrifugal force, and the gravitational vector, $\boldsymbol{u}=[u_1,\ u_2,\ u_3,\ u_4]^{\mathrm{T}}$ is the input vector, and $\boldsymbol{S}\in\mathbb{R}^{7\times4}$ is the driving matrix and is defined as

$$\boldsymbol{S}=\begin{bmatrix} 0 & -1 & 0 & 0\\ 1 & 0 & 0 & 0\\ -1 & 1 & 0 & 0\\ 0 & 0 & 1 & 0\\ 0 & 0 & 0 & 1\\ 0 & 0 & 0 & 0\\ 0 & 0 & 0 & 0 \end{bmatrix} \ldots\ldots\ldots (2)$$

$\boldsymbol{J}_c(\boldsymbol{q})\in\mathbb{R}^{N\times7}$ is the Jacobian matrix and is determined according to the constraint conditions of the robot and N is the number of constraint conditions. $\boldsymbol{\lambda}\in\mathbb{R}^N$ is the constraint force vector given by

$$\boldsymbol{\lambda}=-\boldsymbol{X}(\boldsymbol{q})^{-1}(\boldsymbol{J}_c(\boldsymbol{q})\boldsymbol{M}(\boldsymbol{q})^{-1}\boldsymbol{\Gamma}(\boldsymbol{q},\dot{\boldsymbol{q}},\boldsymbol{u})+\dot{\boldsymbol{J}}_c(\boldsymbol{q},\dot{\boldsymbol{q}})\dot{\boldsymbol{q}}), \quad (3)$$

where

$$\boldsymbol{X}(\boldsymbol{q})=\boldsymbol{J}_c(\boldsymbol{q})\boldsymbol{M}(\boldsymbol{q})^{-1}\boldsymbol{J}_c(\boldsymbol{q})^{\mathrm{T}}, \quad (4)$$

$$\boldsymbol{\Gamma}(\boldsymbol{q},\dot{\boldsymbol{q}},\boldsymbol{u})=\boldsymbol{S}\boldsymbol{u}-\boldsymbol{H}(\boldsymbol{q},\dot{\boldsymbol{q}}). \quad (5)$$

2.2. Constraint conditions

Since the contact point of the biped robot is constrained with ground, constraint equations are expressed as

$$R(\cos\theta_1-1)\dot{\theta}_1+\dot{x}_1=0, \quad (6)$$

$$-R\sin\theta_1\dot{\theta}_1+\dot{z}_1=0. \quad (7)$$

From these equations, we obtain $\boldsymbol{J}_c(\boldsymbol{q})\in\mathbb{R}^{2\times7}$ and $\dot{\boldsymbol{J}}_c(\boldsymbol{q},\dot{\boldsymbol{q}})\in\mathbb{R}^{2\times7}$ as

$$\boldsymbol{J}_c(\boldsymbol{q})\dot{\boldsymbol{q}}=\begin{bmatrix} R(\cos\theta_1-1) & 0 & 0 & 0 & 0 & 1 & 0\\ -R\sin\theta_1 & 0 & 0 & 0 & 0 & 0 & 1 \end{bmatrix}\dot{\boldsymbol{q}}=\boldsymbol{0}_{2\times1}, \quad (8)$$

$$\dot{\boldsymbol{J}}_c(\boldsymbol{q},\dot{\boldsymbol{q}})=\begin{bmatrix} -R\dot{\theta}_1\sin\theta_1 & 0 & 0 & 0 & 0 & 0 & 0\\ -R\dot{\theta}_1\cos\theta_1 & 0 & 0 & 0 & 0 & 0 & 0 \end{bmatrix}. \quad (9)$$

2.3. Impact equation

It is assumed that the collision of the swing-leg with the ground is inelastic and instantaneous. The velocity can thus be derived immediately after impact by solving the impact equations described as follows. As the contact point of the biped robot is constrained with the ground at the collision of the swing-leg, the constraint equations can be expressed as

$$2b_1C_1\dot{\theta}_1-(2b_2-R)C_2\dot{\theta}_2+2S_1\dot{b}_1-2S_2\dot{b}_2+\dot{x}_1=R\dot{\theta}_2, \quad (10)$$

$$-2b_1S_1\dot{\theta}_1+(2b_2-R)S_2\dot{\theta}_2+2\dot{b}_1C_1-2\dot{b}_2C_2+\dot{z}_1=0. \quad (11)$$

where C_1 is $\cos\theta_1$, C_2 is $\cos\theta_2$, S_1 is $\sin\theta_1$ and S_2 is $\sin\theta_2$. From these equations, the instantaneous constraint matrix $\boldsymbol{J}_I(\boldsymbol{q})\in\mathbb{R}^{2\times7}$ is given by

$$\boldsymbol{J}_I(\boldsymbol{q})=\begin{bmatrix} J_{11} & J_{12} & 0 & 2S_1 & -2S_2 & 1 & 0\\ J_{21} & J_{22} & 0 & 2C_1 & -2C_2 & 0 & 1 \end{bmatrix}, \quad (12)$$

where $J_{11}=2b_1C_1$, $J_{12}=-(2b_2-R)C_2-R$, $J_{21}=-2b_1S_1$, and $J_{22}=(2b_2-R)S_2$.

An impulse vector, $\boldsymbol{\lambda}_I\in\mathbb{R}^{N_I}$, and a velocity vector, $\dot{\boldsymbol{q}}^+\in\mathbb{R}^7$, immediately after the impact are given by

$$\boldsymbol{\lambda}_I=-\boldsymbol{X}_I(\boldsymbol{q})^{-1}\boldsymbol{J}_I(\boldsymbol{q})\dot{\boldsymbol{q}}^-, \quad (13)$$

$$\dot{\boldsymbol{q}}^+=(\boldsymbol{I}_{7\times7}-\boldsymbol{M}(\boldsymbol{q})^{-1}\boldsymbol{J}_I(\boldsymbol{q})^{\mathrm{T}}\boldsymbol{X}_I(\boldsymbol{q})^{-1}\boldsymbol{J}_I(\boldsymbol{q}))\dot{\boldsymbol{q}}^-, \quad (14)$$

where $\boldsymbol{X}_I(\boldsymbol{q}) = \boldsymbol{J}_I(\boldsymbol{q})\boldsymbol{M}(\boldsymbol{q})^{-1}\boldsymbol{J}_I(\boldsymbol{q})^{\mathrm{T}}$, $\dot{\boldsymbol{q}}^- \in \mathbb{R}^7$ is the velocity vector immediately before impact, and N_I is the number of instantaneous constraint conditions at impact. The biped robot then changes its stance-leg immediately after impact and the state vector of the robot immediately after the impact is reset to

$$\begin{bmatrix}\boldsymbol{q}^{\mathrm{T}} \\ \dot{\boldsymbol{q}}^{\mathrm{T}}\end{bmatrix} = \begin{bmatrix}\theta_2 & \theta_1 & \theta_3 & b_2 & b_1 & Q_{16} & Q_{17} \\ \dot{\theta}_2^+ & \dot{\theta}_1^+ & \dot{\theta}_3^+ & -\dot{b}_2^+ & -\dot{b}_1^+ & Q_{26} & Q_{27}\end{bmatrix}, \quad (15)$$

where the superscript "+", indicate those immediately after impact due to Eq. (14), $Q_{16} = R(\theta_1 - S_1)$, $Q_{17} = R(1-C_1)$, $Q_{26} = R(1-C_1)\dot{\theta}_1^+$, $Q_{27} = RS_1\dot{\theta}_1^+$.

3. CONTROL METHODS

3.1. Input-output linearization

The low-dimensional dynamic equation of the biped robot for input-output linearization is defined below. The low-dimensional dynamic equation of the biped robot (Fig. 3) when the contact point is always constrained by rotational constraints is given as

$$\boldsymbol{M}_L(\boldsymbol{q}_L)\ddot{\boldsymbol{q}}_L + \boldsymbol{H}_L(\boldsymbol{q}_L, \dot{\boldsymbol{q}}_L) = \boldsymbol{S}_L\boldsymbol{u}, \quad \ldots\ldots (16)$$

where $\boldsymbol{q}_L = [\theta_1,\ \theta_2,\ \theta_3,\ b_1,\ b_2]^{\mathrm{T}}$ is the generalized coordinate vector, $\boldsymbol{M}_L(\boldsymbol{q}_L) \in \mathbb{R}^{5\times5}$ is the inertia matrix, $\boldsymbol{H}_L(\boldsymbol{q}_L, \dot{\boldsymbol{q}}_L) \in \mathbb{R}^5$ is the vector that consists of the Coriolis, centrifugal force and gravitational vector, $\boldsymbol{u} = [u_1,\ u_2,\ u_3,\ u_4]^{\mathrm{T}}$ is the input vector, $\boldsymbol{S}_L \in \mathbb{R}^{5\times4}$ is the driving matrix and is detailed as

$$\boldsymbol{S}_L = \begin{bmatrix} 0 & -1 & 0 & 0 \\ 1 & 0 & 0 & 0 \\ -1 & 1 & 0 & 0 \\ 0 & 0 & 1 & 0 \\ 0 & 0 & 0 & 1 \end{bmatrix}. \quad \ldots\ldots (17)$$

The control output is defined as

$$\boldsymbol{y} = \begin{bmatrix} -\theta_1 + \theta_2 - \phi_d \\ \theta_3 - \theta_{3d} \\ b_1 - b_{1d} \\ b_2 - b_{2d} \end{bmatrix} \to \boldsymbol{0}_{4\times1}. \quad \ldots\ldots (18)$$

$\ddot{\boldsymbol{y}}$ is then obtained by

$$\begin{aligned}\ddot{\boldsymbol{y}} &= \begin{bmatrix} -1 & 1 & 0 & 0 & 0 \\ 0 & 0 & 1 & 0 & 0 \\ 0 & 0 & 0 & 1 & 0 \\ 0 & 0 & 0 & 0 & 1 \end{bmatrix} \ddot{\boldsymbol{q}}_L \\ &= \boldsymbol{T}\ddot{\boldsymbol{q}}_L \\ &= \boldsymbol{T}\boldsymbol{M}_L(\boldsymbol{q}_L)^{-1}(\boldsymbol{S}_L\boldsymbol{u} - \boldsymbol{H}_L(\boldsymbol{q}_L, \dot{\boldsymbol{q}}_L)), \quad \ldots\ldots (19)\end{aligned}$$

where ϕ_d is the desired hip-joint angle, θ_{3d} is the desired torso angle, b_{1d} is the desired length of the b_1 and b_{2d} is the desired length of the b_2. The control input for achieving input-output linearization $\ddot{\boldsymbol{y}} = \boldsymbol{v}$ is given by

$$\boldsymbol{u} = (\boldsymbol{T}\boldsymbol{M}_L(\boldsymbol{q}_L)^{-1}\boldsymbol{S}_L)^{-1}\boldsymbol{A}_1(\boldsymbol{v}, \boldsymbol{q}_L, \dot{\boldsymbol{q}}_L), \quad \ldots\ldots (20)$$

where $\boldsymbol{A}_1(\boldsymbol{v}, \boldsymbol{q}_L, \dot{\boldsymbol{q}}_L) = \boldsymbol{v} + \boldsymbol{T}\boldsymbol{M}_L(\boldsymbol{q}_L)^{-1}\boldsymbol{H}_L(\boldsymbol{q}_L, \dot{\boldsymbol{q}}_L)$ and $\boldsymbol{v} = [v_1,\ v_2,\ v_3,\ v_4]^{\mathrm{T}}$ is the new input vector for the desired motions.

3.2. Stance-leg and torso control

It was first shown that the control methods for the telescopic stance-leg and torso posture were appropriate for level ground walking. Level ground walking of the biped robot was achieved using the following simple PD-control methods:

$$v_2 = -K_{P2}(\theta_3 - \theta_{3d}) - K_{D2}\dot{\theta}_3, \quad (21)$$

$$v_3 = -K_{P3}(b_1 - b_{1d}) - K_{D3}\dot{b}_1, \quad (22)$$

where K_{P2}, K_{P3}, K_{D2} and K_{D3} are the control gains. The biped robot can maintain the desired torso angle by Eq. (21) and the desired length of the stance-leg by Eq. (22).

3.3. Swing-leg control

The control method for achieving swing-leg motion was then designed. Fig. 4 shows the schematic for a biped walking with a long stride. The swing-leg motion is synchronized with the stance-leg angle during dynamic walking. It is thus determined that the desired trajectory of the swing-leg motion of the biped robot is a function of the stance-leg angle like the previous research [16].

The stance-leg angle was redefined as $\theta_v = \theta_1 - \theta_1^s$ where θ_1^s is the stance-leg angle immediately after the stance-leg exchange. The desired trajectory functions are given by

$$\phi_d(\theta_v) = A_3\theta_v^3 + A_2\theta_v^2 + A_0, \quad (23)$$

$$b_{2d}(\theta_v) = B_3\theta_v^3 + B_2\theta_v^2 + B_0. \quad (24)$$

The boundary conditions are defined as $\phi_d(0) = \phi^s$, $\phi_d(\theta_v^t) = \phi^t$, $\dot{\phi}_d(0) = \dot{\phi}_d(\theta_v^t) = 0$ and $b_{2d}(0) = b_2^s$, $b_{2d}(\theta_v^t) = b_2^t$, $\dot{b}_{2d}(0) = \dot{b}_d(\theta_v^t) = 0$, for each coefficient in Eqs. (23) and (24) are given by the following:

$$\begin{aligned} A_3 &= -2(\phi^t - \phi^s)/(\theta_v^t)^3, & A_2 &= 3(\phi^t - \phi^s)/(\theta_v^t)^2, \\ A_0 &= \phi^s, & B_3 &= -2(b_2^t - b_2^s)/(\theta_v^t)^3, \\ B_2 &= 3(b_1^t - b_2^s)/(\theta_v^t)^2, & B_0 &= b_2^s, \end{aligned}$$

where the superscript, "s", indicates the starting value

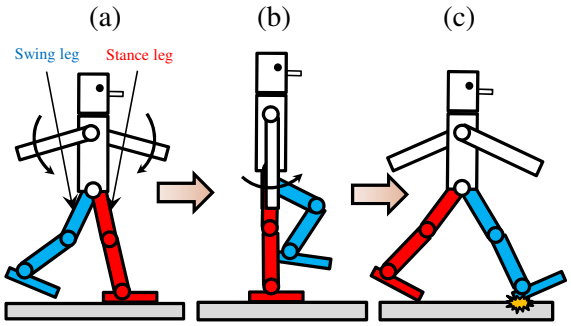

Fig. 4. Schematic for biped walking with long stride

and the superscript, "t", indicates the terminal value. These control methods are given by

$$v_1 = -K_{P1}(\theta_2 - \theta_1 - \phi_d) - K_{D1}(\dot{\theta}_2 - \dot{\theta}_1 - \dot{\phi}_d), \quad (25)$$

$$v_4 = -K_{P4}(b_2 - b_{2d}) - K_{D4}(\dot{b}_2 - \dot{b}_{2d}), \quad (26)$$

where K_{P1}, K_{P4}, K_{D1} and K_{D4} are the control gains and ϕ_d is the desired trajectory of the hip joint angle according to Eq. (23). b_{2d} is the desired trajectory of the length of the b_2 according to Eq. (24). To lock the angle of the hip joint and the length of the swing-leg at the desired values, ϕ_d and $\dot{\phi}_d$ become $\phi_d = \phi_t$ and $\dot{\phi}_d = 0$ when $\theta_2 - \theta_1 \leq \phi^t + 0.001$ is satisfied. b_{2d} and $\dot{b}_{2d}$ then become $b_{2d} = 0.5$ and $\dot{b}_{2d} = 0$ when $b_2 \geq 0.499$ is satisfied.

Fig.5 shows the schematic for the trajectory of swing-leg mass point. Here: (a) the start point, is the point immediately after the stance-leg exchange: (b) pass point, is the point at the minimum length of the swing-leg: and (c) terminal point, is the point immediately before the next stance-leg exchange. We thus design the b_{2d} from (a) to (b) and from (b) to (c) by Eq. (24).

4. WALKING ANALYSIS

4.1. Numerical analysis

Table 1 lists the physical parameters of the biped robot and Table 2 lists the control parameters where the b_2^p is the minimum length of the b_2.

Fig. 6 plots a stick diagram for the limit cycle walking with $\theta_1^p = 0$ rad in a step where θ_1^p is the control parameter for pass point at $b_2 = b_2^p$. Fig. 7 shows the length of b_2 and the input for walking for 3 steps under the actuator torque and force limit (the torque limit is 200 Nm and force limit is 600 N) and Fig. 8 shows the extended figure of the torque. It can be seen that the biped robot achieves limit cycle walking.

Specific resistance (SR) is used as an index for energy-efficiency in the simulations. The SR is an index of

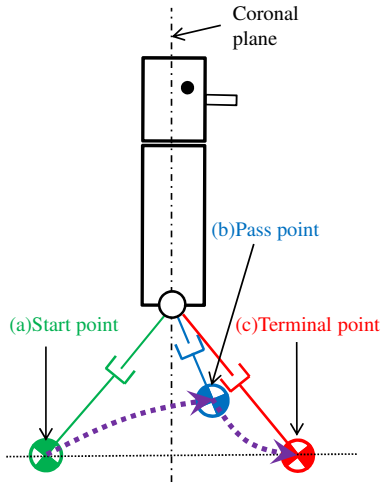

Fig. 5. Schematic for trajectory of swing-leg mass point

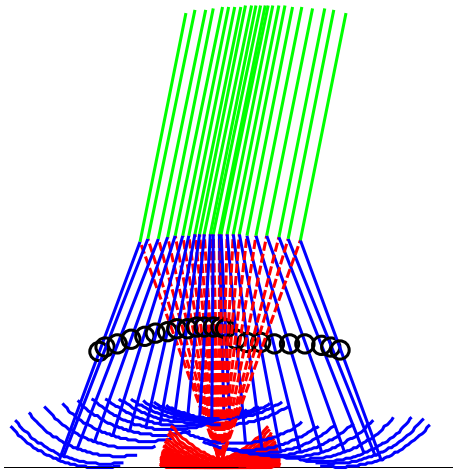

Fig. 6. Stick diagram of dynamic walking where $\theta_1^p = 0$ rad

energy-efficiency in dynamic walking given by

$$\mathrm{SR} := \frac{p}{Mgv}, \quad (27)$$

where p [J/s] is the average input power, M [kg] is the total mass of the robot and v [m/s] is the average walking speed. Average input power, p, is given by

$$p := \frac{1}{T}\int_0^T (|P_1|+|P_2|+|P_3|+|P_4|)\,dt, \quad (28)$$

where $P_1 = u_1(\dot{\theta}_2 - \dot{\theta}_3)$, $P_2 = u_2(\dot{\theta}_3 - \dot{\theta}_1)$, $P_3 = u_3\dot{b}_1$, $P_4 = u_4\dot{b}_2$, and T [s] is the total walking time.

Fig. 9 shows the walking speed, the step period, and

Table 1. Physical parameters

Symbol	Value
b_3	0.5 m
R	0.5 m
m_1	5.0 kg
m_2	5.0 kg
m_h	5.0 kg

Table 2. Control parameters

Symbol	Value	Symbol	Value
K_{P1}	100000 N·m/rad	K_{D1}	2000 N·m/(rad/s)
K_{P2}	50000 N·m/rad	K_{D2}	2500 N·m/(rad/s)
K_{P3}	50000 N/m	K_{D3}	2500 N/(m/s)
K_{P4}	50000 N/m	K_{D4}	2500 N/(m/s)
ϕ_t	−0.70 rad	θ_{3d}	0.20 rad
b_{1d}	0.50 m	b_2^p	0.40 m
b_2^t	0.50 m		

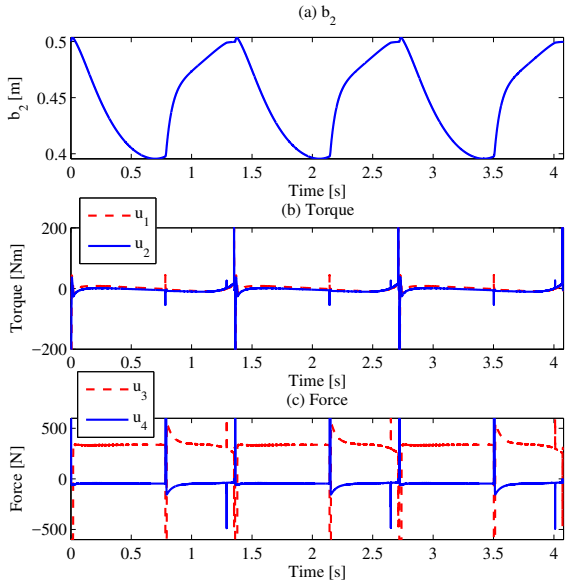

Fig. 7. b_2 and input with respect to time in limit cycle walking

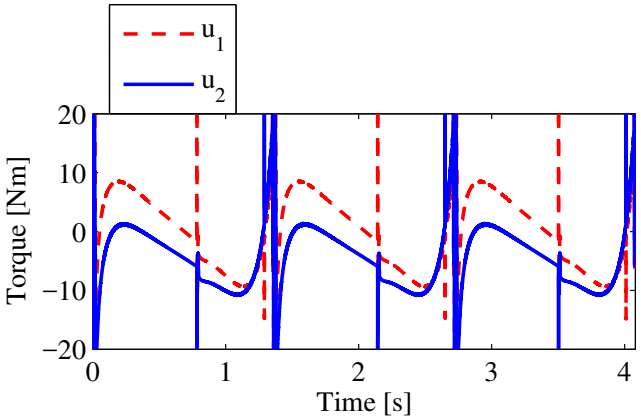

Fig. 8. Torque with respect to time in limit cycle walking where the torque range from -20 to 20 Nm

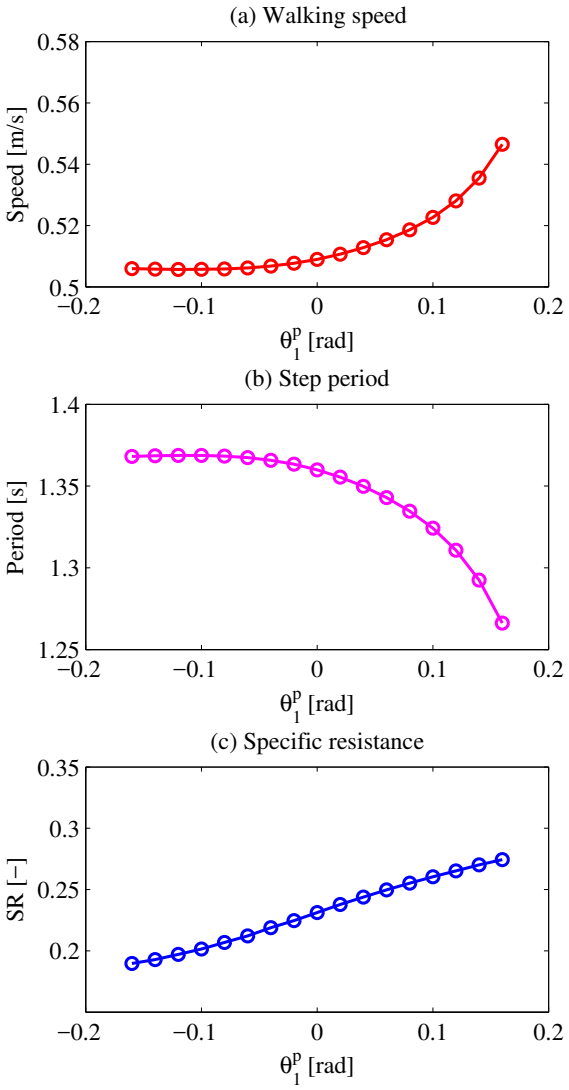

Fig. 9. Walking speed, step period, and SR of limit cycle walking with respect to θ_1^p where $m_1 = 5.0$

the SR for limit cycle walking with respect to θ_1^p. These results show that the walking speed and energy-efficiency depend on the swing-leg trajectory. We can see that the walking speed and SR monotonically increase and the step period monotonically decreases with respect to θ_1^p. The walking speed especially increases when θ_1^p is bigger than 0 [rad].

Fig. 10 plots a stick diagram for limit cycle walking where $\theta_1^p = -0.16$ rad, where the walking speed is the slowest in Fig. 9. Fig. 11 plots a stick diagram for limit cycle walking where $\theta_1^p = 0.16$ rad, where the walking speed is the fastest in Fig. 9. We can see that the swing-leg trajectory where $\theta_1^p = -0.16$ rad considerably differs from the swing-leg trajectory where $\theta_1^p = 0.16$ rad

Moreover, Fig. 12 and Fig. 13 show the walking speed, step period, and SR where $m_1 = 4.0$ kg and $m_1 = 6.0$ kg, respectively. Although the leg mass changes, these property are conserved. The walking speed and SR both monotonically increase and the step period monotonically decreases with respect to θ_1^p.

It is inferred that the asymmetric swing-leg trajectory when the mass point of the swing-leg is raised at a positive stance-leg angle has propulsive effects for speeding-up the pace of walking. To show this principle of propulsive effects, the asymmetric swing-leg motions are mathematically analyzed in the next section.

4.2. Mathematical analysis

The reaction force owing to the swing-leg motion showing the propulsive effect of the asymmetric swing-leg trajectory was analyzed. $\boldsymbol{r}$ is defined as the position

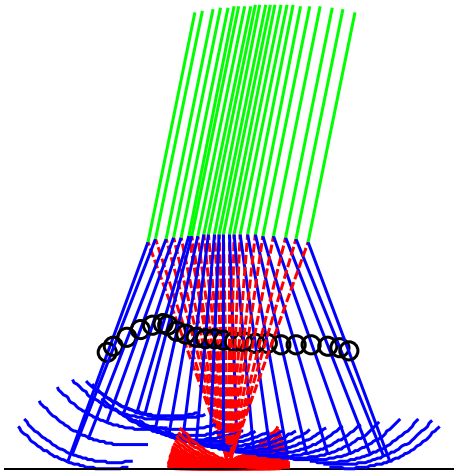

Fig. 10. Stick diagram of dynamic walking where $\theta_1^p = -0.16$ rad

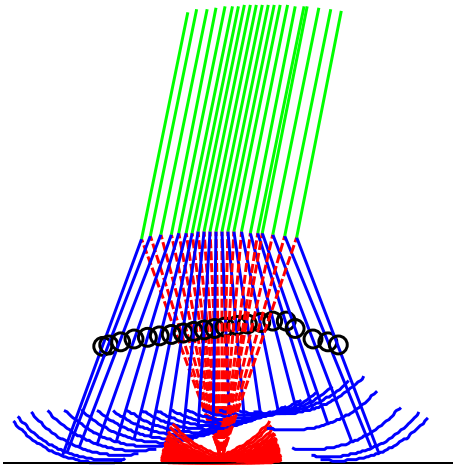

Fig. 11. Stick diagram of dynamic walking where $\theta_1^p = 0.16$ rad

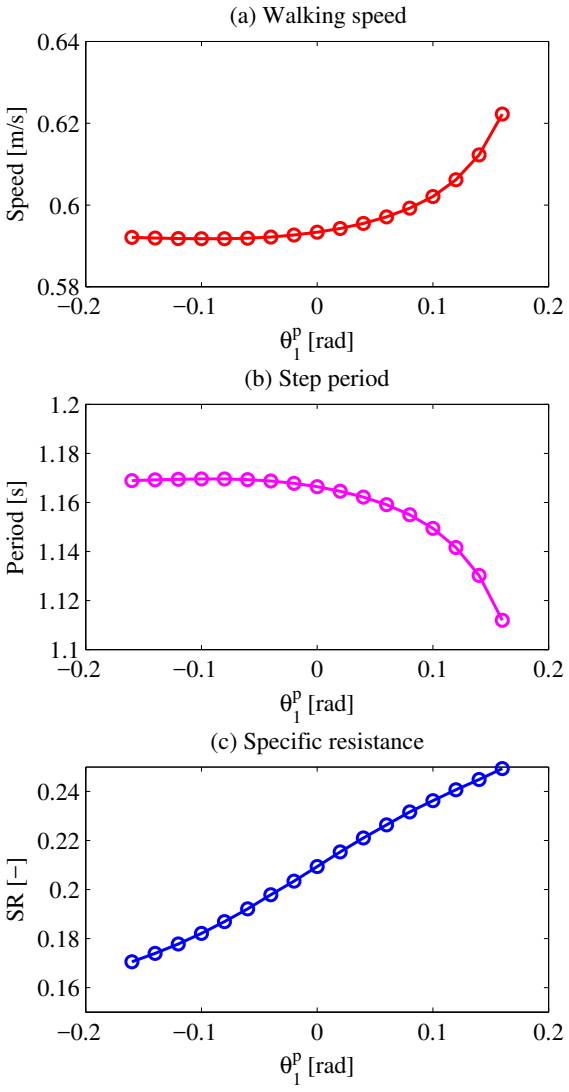

Fig. 12. Walking speed, step period and SR of limit cycle walking with respect to θ_1^p where $m_1 = 4.0$

vector from the contact point to the mass point of hip (m_h), and $\boldsymbol{F}$ is the reaction force vector owing to lengthen and contract the swing-leg. We thus see that the reaction force owing to the swing-leg generates moment at the contact point of the stance-leg that as given by

$$\boldsymbol{M} = \boldsymbol{r} \times \boldsymbol{F}, \quad \ldots\ldots\ldots\ldots\ldots\ldots (29)$$

where this moment is around Y-axis moment.

Fig. 14 shows the moment owing to the reaction force when the swing-leg contracts. The reaction force at the positive stance-leg angle generates a clockwise moment around the contact point. These moments generate a propulsive effect when the angle of the stance-leg is positive but do not generate propulsive effects when the angle of the stance-leg is negative. Fig. 15 shows the moments owing to the reaction force when the swing-leg lengthens. These moments generate a propulsive effect when the angle of the stance-leg is negative but do not generate a propulsive effects when the angle of the stance-leg is positive.

Fig. 16 shows a schematic for the both symmetric and asymmetric swing-leg motion. It can be seen that symmetric swing-leg motion in Fig. 16(a) always generates negative torque from the left side in Fig. 14 and the right side in Fig. 15 whereas asymmetric swing-leg motions as shown in Fig. 16(b) generates a positive torque for a rising swing-leg mass when $\theta_1 > 0$. If it is assumed that the angle of the stance-leg monotonically increases, then the change in mechanical energy can be defined by

$$E = \int_{T_1}^{T_2} |\boldsymbol{r} \times \boldsymbol{F}| \dot{\theta}_1 dt, \quad \ldots\ldots\ldots\ldots (30)$$

where T_1 is the start time for contraction of the swing-leg

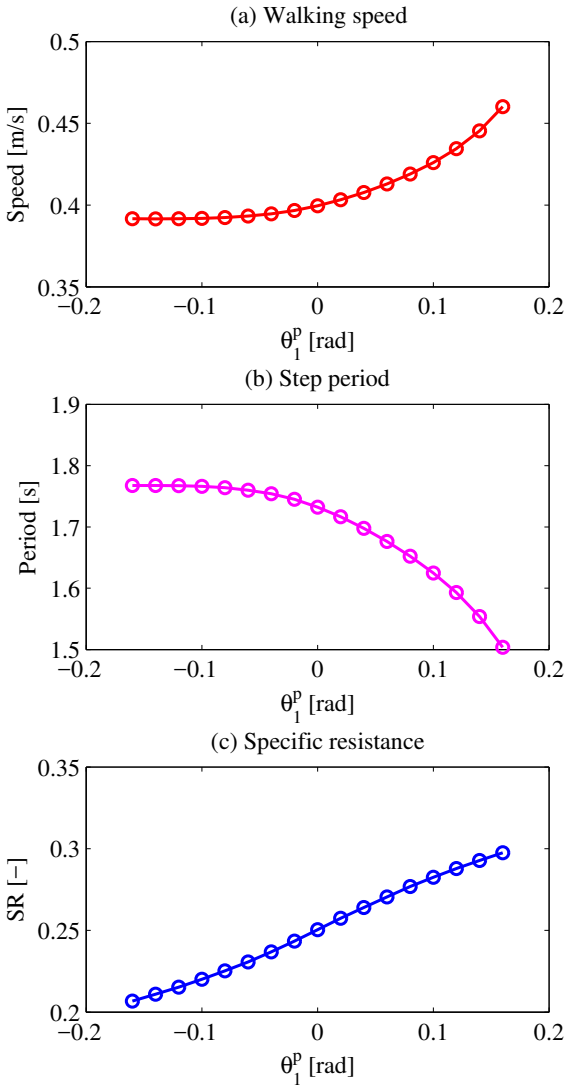

Fig. 13. Walking speed, step period and SR of limit cycle walking with respect to θ_1^p where $m_1 = 6.0$

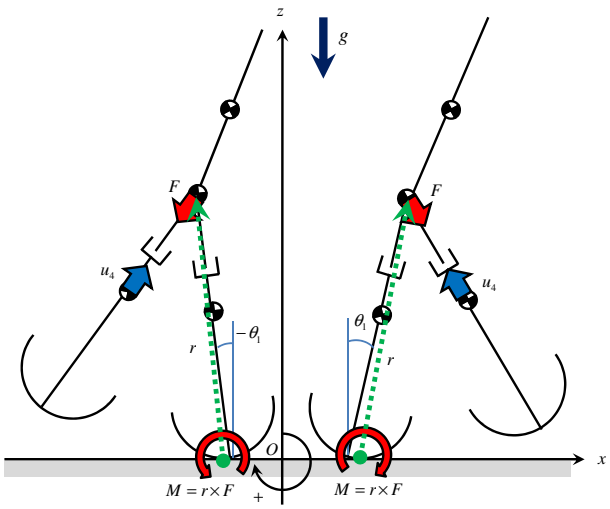

Fig. 14. Reaction force owing to contracted swing-leg

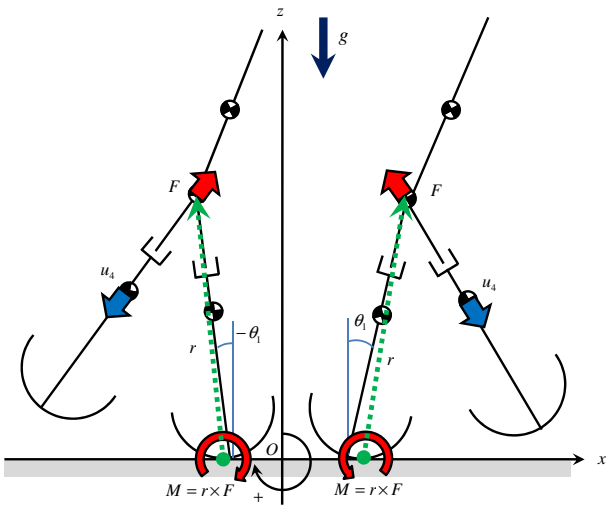

Fig. 15. Reaction force owing to lengthened swing-leg

in the positive stance-leg angle, T_2 is the end time for the contraction of swing-leg. It can be seen that the asymmetric swing-leg motion by this method can generate positive energy. From this result, it is considered that the walking speed in Fig. 9 monotonically increases with respect to an increasing θ_1^p in $\theta_1^p > 0$.

4.3. Design of the asymmetric swing-leg trajectory based on the principle

This principle verification of asymmetric swing-leg motion for high-speed walking was obtained by numerical and mathematical analysis. The asymmetric swing-leg motion was then designed using this principle. The desired trajectory for b_2 was considered at the two pass points P_1 and P_2 as shown in Fig.17. P_1 is the pass point when the stance leg is vertical and P_2 is the pass point when the biped robot maximizes the contraction of the swing-leg. We thus designed the desired trajectory according to the two pass points by Eq.(24).

The biped robot must minimize the contraction of the swing-leg from the start point to P_1 since the contracting swing-leg from the start point to P_1 cause a decreasing walking speed as shown in Fig. 14. However, P_1 must also be set to avoid scuffing of the tip of the leg with ground. Moreover, the biped robot increases the contracting swing-leg from P_1 to P_2 since the contracting swing-leg from P_1 to P_2 causes an increase in walking speed as shown in Fig. 14.

Table 3 lists the control parameters where the θ_1^{P1} and b_2^{P1} are the parameters relating to the P_1 and θ_1^{P2} and b_2^{P2} are parameters relating to the P_2.

Fig. 18 shows the walking speed, walking period, and SR with respect to K_ϕ where K_ϕ is the control parameter in Table 3. When K_ϕ is big value, the biped robot

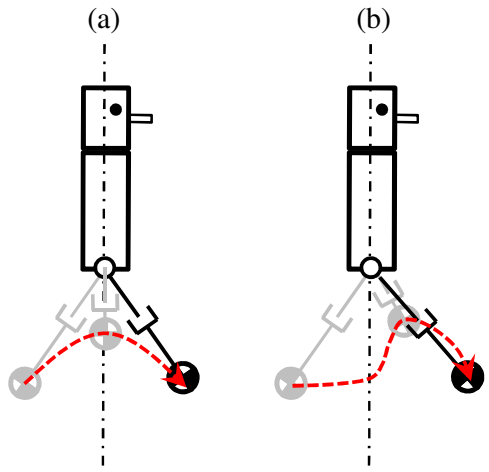

Fig. 16. Schematic for symmetric and asymmetric swing-leg trajectories

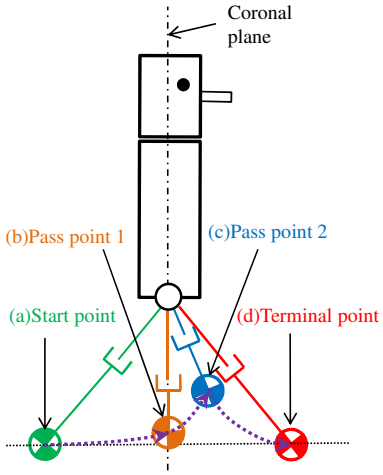

Fig. 17. Schematic for swing-leg mass point for redesign asymmetric trajectory

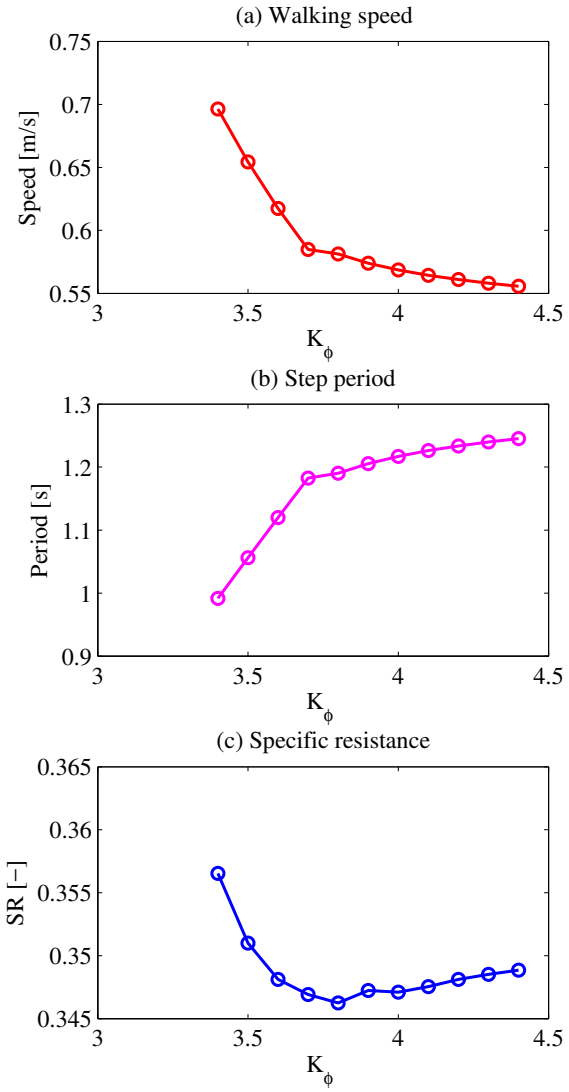

Fig. 18. Walking speed, step period, and SR of limit cycle walking with respect to K_ϕ

quickly raises the swing-leg. It can be seen that the walking speed monotonically increases with a decreasing K_ϕ value. However, It can also be seen that SR does not considerably change with respect to a changing walking speed. Fig. 19 shows a stick diagram for limit cycle walking where $K_\phi = 3.4$, and Fig. 20 shows the inputs for limit cycle walking. Fig. 21 shows extended figure of torque. The walking speed is at a maximum in Fig. 18 and it can be seen that the swing-leg trajectory in this example is asymmetric. Therefore, the speed of limit cycle walking using asymmetric swing-leg trajectories can be improved for biped robots based on the principle.

Table 3. Control parameters for b_2

Symbol	Value	Symbol	Value
θ_1^{P1}	0.00 rad	b_2^{P1}	0.49 m
θ_1^{P2}	ϕ^t/K_ϕ rad	$b_2^{P2}(=b_2^p)$	0.40 m

5. CONCLUSION AND FUTURE WORK

In this study, a novel method for increasing the speed of limit cycle walking for biped robots using asymmetric swing-leg motions has been demonstrated. It was first shown that the swing-leg motion has an impact on the walking speed by using numerical simulations. It

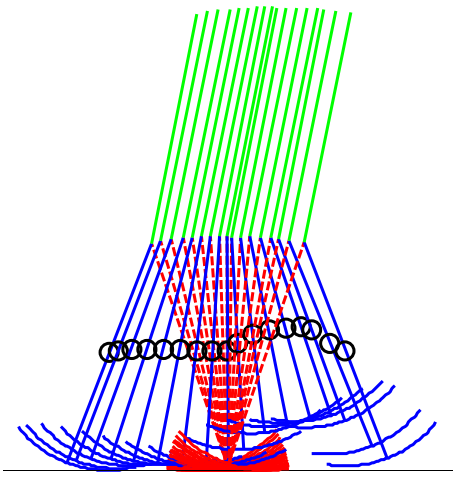

Fig. 19. Stick diagram of limit cycle walking with redesigned asymmetric swing-leg motion

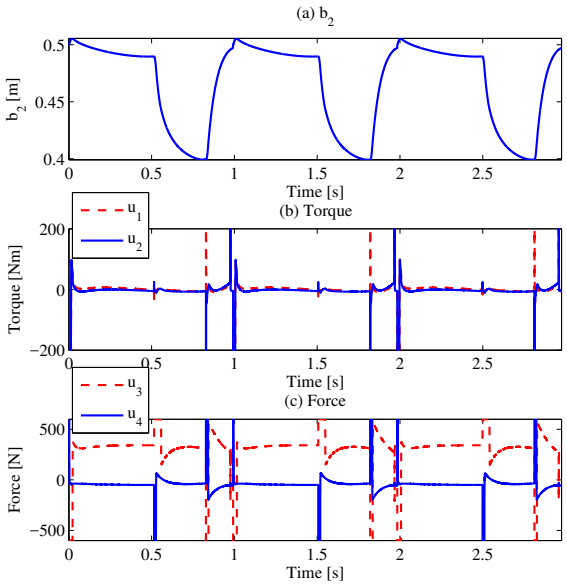

Fig. 20. b_2 and input with respect to time in limit cycle walking

was then proven mathematically that the contraction and lengthening of swing-leg motions generates torque for producing propulsive effects. Moreover, it was shown that the biped robot can achieve a high walking speed by employing asymmetric swing-leg motion based on this principle. Future work plans to verify the effectiveness of this proposed method by experimental trials and extend this method to biped robots with knees.

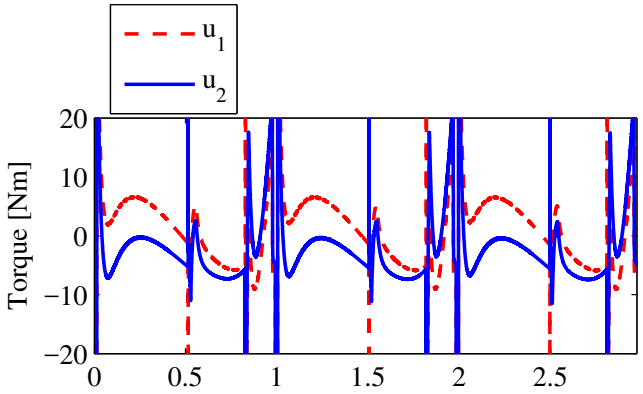

Fig. 21. Torque with respect to time in limit cycle walking where the torque range from -20 to 20 Nm

Acknowledgements

This work was supported by JSPS KAKENHI Grant-in-Aid for Young Scientists (B) Grant Number 15K18090.

References:

[1] HONDA,"Humanoid Robot ASIMO," Supporting Online Materials

[2] PETMAN, "Boston dynamics: Humanoid robot petman," Supporting Online Materials

[3] S.H.Collins and A. Ruina, "A bipedal walking robot with efficient and human-like gait," in Proc. IEEE international conference on robotics and automation (ICRA). pp.1983–1988, 2005

[4] T. McGeer, "Passive dynamic walking," The International Journal of Robotics Research, vol.9, no.2, pp.62–82,1990.

[5] D.G.E. Hobbelen and M. Wisse, "Limit cycle walking", Humanoid Robots, Human-like Machines, chapter 14. InTech, 2007.

[6] F. Asano, M. Yamakita, and K. Furuta, Virtual passive dynamic walk- ing and energy-based control laws, " in Proc. IEEE/RSJ International Conference on Intelligent Robots and Systems (IROS), pp. 1149–1154, 2002.

[7] F. Asano, M. Yamakita, N. Kamamichi, and Z.W. Luo, "A novel gait generation for biped walking robots based on mechanical energy constraint," IEEE Transactions on Robotics and Automation, vol.20, no.3, pp.565–573, 2004.

[8] M. Wisse and J.Van Frankenhuyzen, "Design and construction of mike; a 2d autonomous biped based on passive dynamic walking," in Proc. International Symposium of Adaptive Motion and Animals and Machines (AMAM03), 2003.

[9] M. Wisse,"Three additions to passive dynamic walking; actuation, an upper body, and 3D stability, " in Proc. IEEE/RAS International Conference on Humanoid Robots (Humanoids), vol. 1, pp. 113–132, 2004.

[10] T. Narukawa, M. Takahashi, and K. Yoshida, "Biped locomotion on level ground by torso and swing-leg control based on passive-dynamic walking," in Proc. IEEE/RSJ International Conference on Intelligent Robots and Systems (IROS), pp.4009–4014, 2005.

[11] F. Asano and Z.W. Luo, "Energy-efficient and high-speed dynamic biped locomotion based on principle of parametric excitation," IEEE Transactions on Robotics, vol.24, no.6, pp.1289–1301,2008.

[12] T. Kinugasa, S. Miwa and K. Yoshida, "Frequency analysis for biped walking via leg length variation," Journal of Robotics and Mechatronics, vol.20, no. 1, pp. 98–105, 2008.

[13] Y. Hanazawa, T. Hayashi, M. Yamakita and F. Asano, "High-speed limit cycle walking for biped robots using active up-and-down motion control of wobbling mass," in Proc. IEEE/RSJ International Conference on Intelligent Robots and Systems (IROS), pp.3649–3654, 2013.

[14] Y. Hanazawa and F. Asano, "High-speed biped walking using swinging-arms based on principle of up-and-down wobbling mass," in Proc. IEEE International Conference on Robotics and Automation (ICRA), pp.5191–5196, 2015.

[15] F. Iida and R. Tedrake, "Minimalistic control of biped walking in rough terrain," Autonomous Robots, vol.28, no.3, pp.355–368, 2010.

[16] J.W. Grizzle, G. Abba, and F. Plestan, "Asymptotically stable walking for biped robots: Analysis via systems with impulse effects," IEEE Transactions on automatic control, vol.46, no.1,pp.51–64, 2001.

Appendix

$\boldsymbol{M}(\boldsymbol{q})$ matrix and $\boldsymbol{H}(\boldsymbol{q},\dot{\boldsymbol{q}})$ vector in Eq.(1) M_{ij} is i-th row and j-th column element in $\boldsymbol{M}(\boldsymbol{q})$ and H_i is i-th row element in $\boldsymbol{H}(\boldsymbol{q},\dot{\boldsymbol{q}})$.

$M_{11} = b_1^2(5m_1 + 4m_2 + 4m_h)$
$M_{12} = -2b_1b_2m_1\cos(\theta_1 - \theta_2)$
$M_{13} = 2b_1b_3m_2\cos(\theta_1 - \theta_3)$
$M_{14} = 0$
$M_{15} = 2b_1m_1\sin(\theta_1 - \theta_2)$
$M_{16} = b_1\cos\theta_1(3m_1 + 2m_2 + 2m_h)$
$M_{17} = -b_1\sin\theta_1(3m_1 + 2m_2 + 2m_h)$
$M_{21} = M_{12}$
$M_{22} = b_2^2m_1$
$M_{23} = 0$
$M_{24} = -2b_2m_1\sin(\theta_1 - \theta_2)$
$M_{25} = 0$
$M_{26} = -b_2m_1\cos(\theta_2)$
$M_{27} = b_2m_1\sin(\theta_2)$
$M_{31} = M_{13}$
$M_{32} = M_{23}$
$M_{33} = b_3^2m_2$
$M_{34} = 2b_3m_2\sin(\theta_1 - \theta_3)$
$M_{35} = 0$
$M_{36} = b_3m_2\cos\theta_3;$
$M_{37} = -b_3m_2\sin(\theta_3)$
$M_{41} = M_{14}$
$M_{42} = M_{24}$
$M_{43} = M_{34}$
$M_{44} = 5m_1 + 4m_2 + 4m_h$
$M_{45} = -2m_1\cos(\theta_1 - \theta_2)$
$M_{46} = \sin\theta_1(3m_1 + 2m_2 + 2m_h)$
$M_{47} = \cos\theta_1(3m_1 + 2m_2 + 2m_h)$
$M_{51} = M_{15}$
$M_{52} = M_{25}$
$M_{53} = M_{35}$
$M_{54} = M_{45}$
$M_{55} = m_1$
$M_{56} = -m_1\sin\theta_2$
$M_{57} = -m_1\cos\theta_2$
$M_{61} = M_{16}$
$M_{62} = M_{26}$
$M_{63} = M_{36}$
$M_{64} = M_{46}$
$M_{65} = M_{56}$
$M_{66} = 2m_1 + m_2 + m_h$
$M_{67} = 0$
$M_{71} = M_{17}$
$M_{72} = M_{27}$
$M_{73} = M_{37}$
$M_{74} = M_{47}$
$M_{75} = M_{57}$
$M_{76} = M_{67}$
$M_{77} = 2m_1 + m_2 + m_h$

$H_1 = 2b_1(b_3m_2\sin(\theta_1 - \theta_3)\dot{\theta}_3^2 - 2\dot{b}_2m_1\cos(\theta_1 - \theta_2)\dot{\theta}_2 - b_2m_1\sin(\theta_1 - \theta_2)\dot{\theta}_2^2 + 5\dot{b}_1\dot{\theta}_1m_1 + 4\dot{b}_1\dot{\theta}_1m_2 + 4\dot{b}_1\dot{\theta}_1m_h) - b_1g\sin\theta_1(3m_1 + 2m_2 + 2m_h)$

$H_2 = 2b_2m_1(b_1\sin(\theta_1 - \theta_2)\dot{\theta}_1^2 - 2\dot{b}_1\cos(\theta_1 - \theta_2)\dot{\theta}_1 + \dot{b}_2\dot{\theta}_2) + b_2gm_1\sin\theta_2$

$H_3 = 2b_3\dot{\theta}_1m_2(2\dot{b}_1\cos(\theta_1 - \theta_3) - b_1\dot{\theta}_1\sin(\theta_1 - \theta_3)) - b_3gm_2\sin\theta_3$

$H_4 = 2b_2\dot{\theta}_2^2m_1\cos(\theta_1 - \theta_2) - 4b_1\dot{\theta}_1^2m_2 - 4b_1\dot{\theta}_1^2m_h - 4\dot{b}_2\dot{\theta}_2m_1\sin(\theta_1 - \theta_2) - 5b_1\dot{\theta}_1^2m1 - 2b_3\dot{\theta}_3^2m_2\cos(\theta_1 - \theta_3) + g\cos\theta_1(3m_1 + 2m_2 + 2m_h)$

$H_5 = m_1(2b_1\cos(\theta_1 - \theta_2)\dot{\theta}_1^2 + 4\dot{b}_1\sin(\theta 1 - \theta 2)\dot{\theta}_1 - b_2\dot{\theta}_2^2) - gm_1\cos\theta_2$

$H_6 = 6\dot{b}_1\dot{\theta}_1m_1\cos\theta_1 - 2\dot{b}_2\dot{\theta}_2m_1\cos\theta_2 + 4\dot{b}_1\dot{\theta}_1m_2\cos\theta_1 + 4\dot{b}_1\dot{\theta}_1m_h\cos\theta_1 - 3b_1\dot{\theta}_1^2m_1\sin\theta_1 - 2b_1\dot{\theta}_1^2m_2\sin\theta_1 + b_2\dot{\theta}_2^2m_1\sin\theta_2 - b_3\dot{\theta}_3^2m_2\sin\theta_3 - 2b_1\dot{\theta}_1^2m_h\sin\theta_1$

$H_7 = 2\dot{b}_2\dot{\theta}_2m_1\sin\theta_2 - 6\dot{b}_1\dot{\theta}_1m_1\sin\theta_1 - 4\dot{b}_1\dot{\theta}_1m_2\sin\theta_1 - 4\dot{b}_1\dot{\theta}_1m_h\sin\theta_1 - 3b_1\dot{\theta}_1^2m_1\cos\theta_1 - 2b_1\dot{\theta}_1^2m_2\cos\theta_1 + b_2\dot{\theta}_2^2m_1\cos\theta_2 - b_3\dot{\theta}_3^2m_2\cos\theta_3 - 2b_1\dot{\theta}_1^2m_h\cos\theta_1 + g(2m_1 + m_2 + m_h)$

Name:
Yuta Hanazawa

Affiliation:
Dept. of Applied Science for Integrated System Engineering, Graduate School of Engineering, Kyushu Institute of Technology

Address:
1-1 Sensui, Tobata, Kitakytushu, Fukuoka 804-8550, JAPAN
Brief Biographical History:
Your History
Main Works:
• Your Works
Membership in Academic Societies:
• Your Learned Societies

Name:
Fumihiko Asano

Affiliation:
School of Information Science, Japan Advanced Institute of Science and Technology

Address:
1-1 Asahidai, Nomi, Ishikawa 923-1292, JAPAN
Brief Biographical History:
Your History
Main Works:
• Your Works
Membership in Academic Societies:
• Your Learned Societies